The Application of Cloud Texture and Motion derived from Geostationary Satellite Images in Rain Estimation—A Study on Mid-latitude depressions

Aimamorn Suvichakorn and Adrian Tatnall
Astronautics Research Group
School of Engineering Sciences
University of Southampton
Email: aimamorn@soton.ac.uk, art4@soton.ac.uk

***Abstract*— This paper presents the preliminary results of a rain rate estimation system that utilizes a combination of cloud appearance and motion that can be derived from Meteosat7. The proposed rain rate estimation system consists of three steps: feature selection, rain estimation and validation. In feature selection, cloud textural information is extracted and cloud motions are derived by a modified optical flow technique. Next, rain estimation is done using results from a supervised *k-nearest neighbour* (k-NN) classifier. Then, the results when applied to cold front dominated mid-latitude depressions are validated to update the classifier. Finally, the system's performance and its limitation are also discussed.**

I. Introduction

Satellite imagery is routinely used to monitor of large-scale systems e.g. supercell thunderstorms, depressions, cyclones, or mesoscale convective complex, particularly those in remote areas where there are sparse numbers of weather stations. The movement and patterns of clouds, observed from satellite images, can be used to indicate the instabilities of the weather [1]. Hence, their distinct appearances provide some useful information to help rainfall estimation. Together with rain cloud motion, it is also possible to predict the rainfall a short period in advance from satellite imagery or to update a rain estimation.

Geostationary satellite images, though indirectly related to rainfall, are the most promising sources for rainfall information and there is considerable research that demonstrates methods of rainfall estimation [2]. The cloud indexing approach, e.g. Geostationary Operational Environmental Satellite (GOES) Precipitation Index (GPI), is the oldest method and is still useful. It assigns a predetermined rain rate to each cloud type. The technique is simple, yet more stable than other complex methods. However, using only temperature as a basis of rain estimation is valid only for convective rains at coarse spatial and temporal scale. Bi-spectral techniques are based on a relationship between cold-thick clouds i.e. those bright in both conventional infrared (IR) and visible (VIS) images and a high probability of precipitation. However, due to considerable overlaps in the temperature-thickness distribution, O' Sullivan et al. [3] propose a method using brightness and textural characteristics of daytime VIS data and IR temperature patterns to categorise rainfall into no rain, light rain, moderate and heavy rain. Using this method, they achieve 81% accuracy of rain cloud detection, compared to 66% in [4] when no textural characteristics is exploited. However, the work does not relate available texture to rain rate directly. Cloud model-based techniques estimate rain rates as a function of cloud's characteristics, which can be found empirically using radar calibration or numerical weather models. Lensky and Rosenfeld [5] assign rain rates to a mixture of convective clouds and stratiform clouds as a function of updraft velocity, water vapour mixing ratio, cloud droplet's effective radius and air pressure. The effective radius is used as an indicator for large water drops and ice crystals which are the initiation of coalescence precipitation. It can be derived from channel 3 ($3.7\mu m$) of the Advanced Very High Resolution Radiometer (AVHRR) data [5] or from tri-spectral bands at $0.7, 3.7$ and $10.8\mu m$ of the Meteosat Second Generation (MSG) [6].

There is also a more direct method to determine precipitation by using microwave (0.1-10 cm wavelength) radiation which corresponds to precipitation droplet size. Nevertheless, its disadvantages are poor spatial and temporal resolution, together with the difficulties in interpreting the images, especially over land. There are several on-going researches propose hybrid methods combining geostationary satellite data and microwave [7] but how to combine such disparate information at different spatial and temporal scales is still a demanding challenge. At present, active radar observations from the Tropical Rainfall Measuring Mission (TRMM) Precipitation Radar provide the most accurate high resolution satellite-based rainfall estimates [8] but the data are not available at the mid-latitudes area.

This paper focuses on data available from geostationary satellites which includes VIS, IR and water vapour (WV) images and extracts the advantageous data that can relate to rainfall rates.

II. Methodology

The proposed rain approximation consists of 3 stages: feature extraction, rain rate assignment and validation. First,

texture information is quantified and cloud motions are derived. Next, the selected features are fed to supervise a k-NN classifier. In the last stage, the output i.e. assigned rain rates are validated. The error information can be used to guide the classifier for the next approximation. Here, a cold-front dominated cyclone is chosen to study since the system combines both convective and stratiform rains, which are primary types of rainfall.

To extract features, it can be seen that the typical characteristics of a cold-front dominated cyclone observed from satellite is a meridionally elongated spiral. Krennert et al. [9] observes that the cloud spiral is white in VIS, has various gray shades in IR but has the brightest in the transition area where the point of occlusion is found. It also appears white in WV within the frontal cloudiness. At the rear edge (the inner boundary of the spiral), there is a sharp gradient from white to black in WV due to the dry intrusion which causes a preferred area of instability for cumulonimbus development. Ahead of the surface front, the precipitation is broad (5-50 km) with its maximum close to the occlusion point. There may be showers, thunderstorms or even hails at the rear part of the spiral.

In order that all three types of images should be used for the analysis, they have been combined to produce a false image by associating the IR, VIS and WV to the red, green and blue colour bands, respectively. In this way, a pixel is a result of three independent vectors. At night when VIS images are not available, the green color band is substituted by a mixture of 50% IR and 50% WV images. Both types of false images and its corresponded rainfall data from ground radars are shown in Fig. 1 as an example. The illustration shows that the substituted image almost resembles Fig. 1 (a) but has less texture.

The first textural features are means and standard deviations of magnitudes of pixel vectors and angles between the vector and the red-blue plane (θ). Then, we project the vectors on to the red-blue plane and use angles between projected vectors and the blue axis (ϕ) as another type of feartures (see Fig. 3). These first order statistics are used as rotation-invariant representatives of the cloud texture. In addition, ϕ implies a proportion of cloud top temperatures and water contents. This is to identify the location of precipitable clouds whereas θ accounts for amounts of the rainfall through the cloud thickness properties. Next, the relationship between a considered pixel and its neighbours are characterised by an autoco-occurrence, which is defined as a joint probability of gray levels of any two similar pixels separated by a given displacement i.e. 3 and 5 pixels in this paper. These features are a measure of homogeneity within cloud structures and are calculated separately for each colour band.

To represent structural characteristics, a bank of Gabor filters is applied to the false images. The Gabor filter is a complex sinusoidal function modulated by a rotated 2D-Gaussian surface curve with a spread of σ_x and σ_y in $x-$ and $y-$direction. Its real impulse response is given by

$$h(x,y) = \frac{1}{2\pi\sigma_x\sigma_y}\exp(-\frac{1}{2}[\frac{x^2}{\sigma_x^2}+\frac{y^2}{\sigma_y^2}])\cos(2\pi u_0 x) \quad (1)$$

where u_0 is a modulating frequency. The response of each rotating angular angle corresponds to image structure in that direction.

To derive cloud motion, the modified optical flow technique has been used. Horn and Schunck [10] propose the idea of optical flow to derive velocity of an object in three dimensional space from a sequence of 2D images by exploiting a fluid dynamics constraint. This technique pretends to see a connection of the object in two sequential image and describes this invisible connection by (optical) fluid flows. The idea is also analogous to cloud motion, which is a special case of fluid motion and consists of very complex motion dynamics [11]. Following [12], velocity $\vec{\omega}$ can be found by minimising an error function:

$$E(\vec{\omega}) = \int((\nabla I)\cdot\vec{\omega}+I(\nabla\cdot\vec{\omega})+I_t)^2 dxdy+\lambda\int_R(||\nabla\vec{\omega}||^2)dxdy, \quad (2)$$

where I, I_t and λ refer to image intensity, its first derivative with respect to time and a Lagrange multiplier, respectively. Considering the image intensity as density, the equation also matches the mass continuity of the compressible fluids e.g. gases and vapours, which are the main components of clouds and their density depends on the coordinates $\vec{x}$ in space and may depend on time as well. The compressible optical flow approach tends to work well to recover cloud motion, since it utilizes fluid dynamics constraints which are applicable to clouds [12]. The last set of features are differences between the texture features derived from the current image and the previous image in the sequence. The temporal interval between Meteosat7 images are 30 minutes. To illustrate how these parameters can classify rain rates, we map them onto a self-organising map (SOM) [13] of 100 classes. The number of classes is equal to that of the k-NN classifier used for the rain approximation. Fig. 4 shows distances between each class (seen as grid). The brighter areas indicate the more distance, in other words, the two classes can be well-classified.

All described textural features, their deviation from those of the previous 30 minutes image and the derived cloud motion are used to train the k-NN classifier. The number of output clusters are 100, each of which has a predefined rain rate. The k-NN classifier labels an input with the label of the majority of the k nearest neighbours, justified by the smallest Euclidean distance. The classifier should be updated every time that actual rain rates are available for the best accuracy. The derived rain rate is post-processed by comparing with its neighbours. If the difference exceeds a specific threshold, a median rain rate calculated from its neighbour is assigned instead.

Note that the images are first preprocessed using the filters in Fig. 2 to outline details and then normalised.

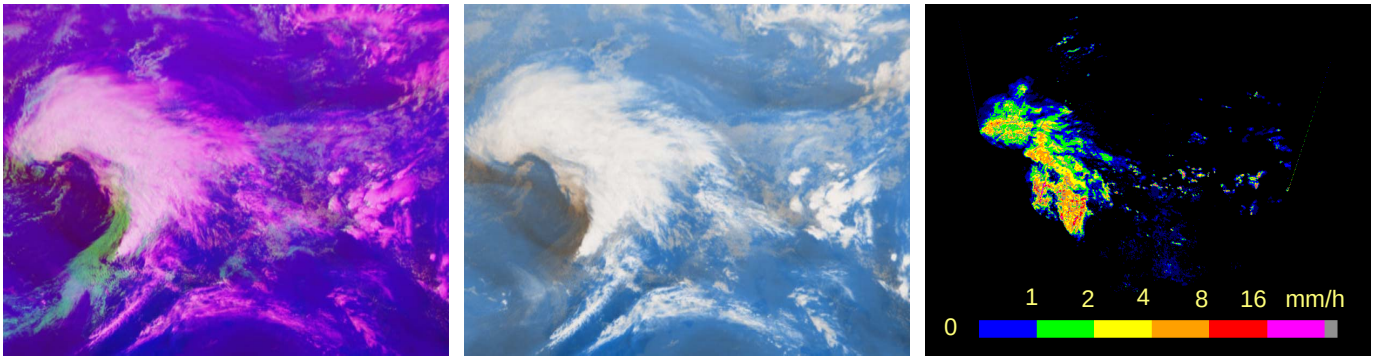

(a) (b) (c)

Fig. 1. False images of a summer mid-latitude depression over the British Isles on 22 June 2004 at 1600GMT from Meteosat7 during daytime (a) and when VIS images are not available (b). The corresponding rain rates are in (c). All images are equidistant projection.

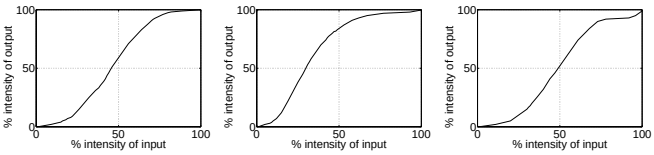

(a) IR (b) VIS (c) WV

Fig. 2. Filters used to preprocess each type of images.

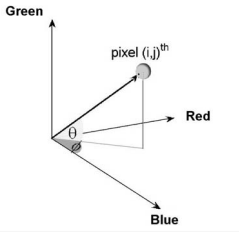

Fig. 3. Colour image axis of a pixel.

III. Analysis

The derived rainfall in Fig. 5 indicates a relevance of the selected features and rain rates. The classifier is also effective at a short period ahead of the time that it is trained. Fig. 6 shows a result when applying the same classifier to approximate rainfalls in the next 2 hours and Fig. 7 illustrates an increase of approximation errors with respect to time. This means that, although the proposed features relate to rainfall, their relationship gradually changes with time. We are currently studying how the relationship changes to make the system more generalised. In the case that the VIS image is not available, Fig. 8 shows that the proposed system can better approximate rainfalls under 12 mm/h than large amounts of rainfalls. The possible reason includes insufficient numbers of the training sets at high rain rates, which appear only at the rear edge of the occlusion.

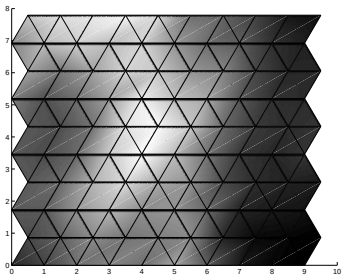

Fig. 4. Distances between 100 classes when classified the features using SOM.

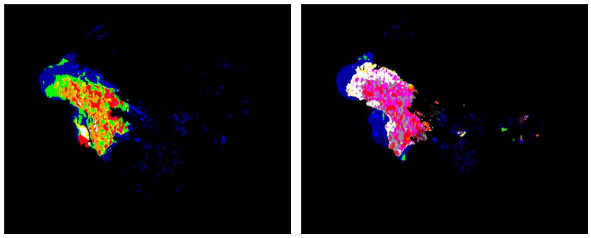

(a) with VIS image (b) without VIS image

Fig. 5. Derived rainfall derived from the false image in Fig. 1 (a).

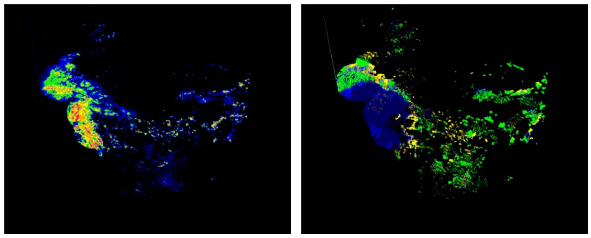

(a) actual rainfall rate (b) derived rainfall rate

Fig. 6. Comparison of the actual rainrate and the predicted rain rate at 2 hours ahead of time,

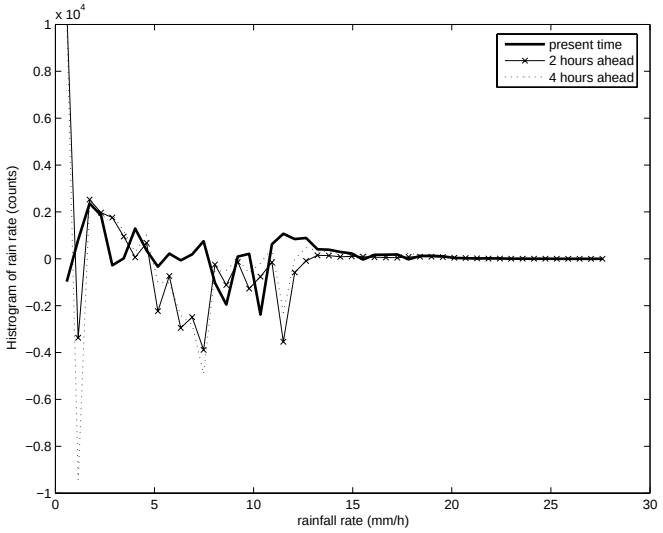

Fig. 7. Errors of the derived rain rates at different time.

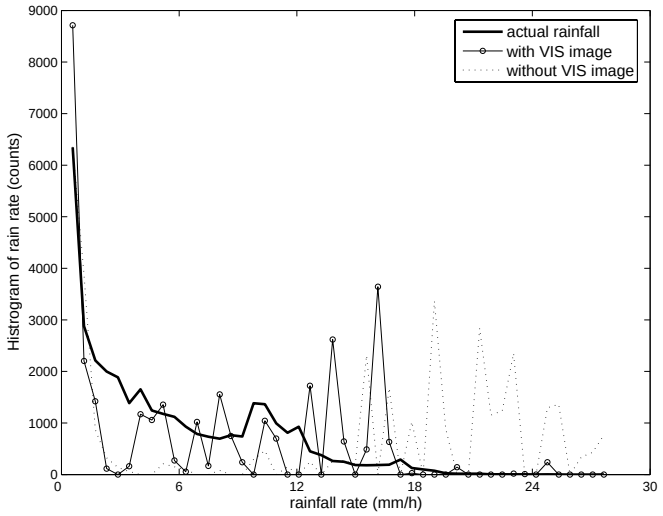

Fig. 8. Histrogram of the derived rain rates, compared to the actual value.

IV. Conclusion

We propose an algorithm to approximate rain rate by using cloud texture and motion derived from Meteosat7. Good agreement, except in cases of very high rainfall, has been found between the predicted rainfall rate and the actual rate measured by ground radars. The best agreement is found when visible, infrared and water vapour imagery are available and the loss of the visible imagery degrades the prediction significantly. However, it can be improved by finding more generalised relation between these features and rain rates. In addition, more features e.g. environment at the surface and cloud microphysics can be included for more accurate results.

Acknowledgment

The authors would like to thank the British Atmospheric Data Centre, the British Meteorological Office and Eumetsat for the data used to process in this paper.

References

[1] M. Bader, G. Forbes, J. Grant, R. Lilley, and A. Waters, *Images in Weather Forecasting-A Practical Guide for Interpreting Satellite and Radar Imagery*. Cambridge: University Press, 1995.

[2] E. C. Barett and D. W. Martin, *The Use of Satellite Data in Rainfall Monitoring*. New York: Academic Press, 1981.

[3] F. O'Sullivan, C. H. Wash, M. Stewart, and C. E. Motell, "Rain estimation from infrared and visible GOES satellite data," *Journal of Applied Meteorology*, vol. 29, no. 3, pp. 209–223, March 1990.

[4] A. A. Tsonis and G. A. Isaac, "On a new approach for instantaneous rain area delineation in the midlatitudes using GOES data," *Journal of Climate and Applied Meteorology*, vol. 24, pp. 1208–1218, November 1985.

[5] I. M. Lensky and D. Rosenfeld, "Estimation of precipitation area and rain intensity based on the microphysical properties retrieved from noaa avhrr data," *Journal of Applied Meteorology*, vol. 36, pp. 234–242, 1997.

[6] C. Reudenbach and J. Bendix, "Satellite based rainfall retrieval with Meteosat, GOES and MSG in the mid-latitudes and the tropics," in *Workshop on Precipitation*, 2002.

[7] C. Kidd, D. R. Kniveton, M. C. Todd, and T. J. Bellerby, "Satellite rainfall estimation using combined passive microwave and infrared algorithms," *Journal of Hydrometeorology*, vol. 4, no. 6, p. 10881104, December 2003.

[8] A. Negri, L. Xu, and R. Adler, "A trmm-calibrated infrared rainfall algorithm applied over brazil," *Journal of Geophysical Research*, vol. 107, no. D20, pp. 8048–8062, September 2002.

[9] T. Krennert, R. Winkler, B. Zeiner, and V. Zwatz-Meise, *Manual of synoptic satellite meteorology conceptual models*, Zentralanstalt für Meteorologie und Geodynamik (ZAMG), Austria, 1999. [Online]. Available: http://www.knmi.nl/samenw/satrep/

[10] B. K. P. Horn and B. G. Schunck, "Determining optical flow," *Artificial Intelligence*, vol. 17, no. 1-3, pp. 185–203, August 1981.

[11] L. Zhou, C. Kambhamettu, and D. B. Goldgof, "Fluid structure and motion analysis from multi-spectrum 2D cloud image sequences," in *Proceedings of IEEE Computer Society Conference on Computer Vision and Pattern Recognition*, vol. 2, South Carolina, June 2000, pp. 744 –751.

[12] D. Béréziat and J.-P. Berroir, "Motion estimation on meteorological infrared data using a total brightness invariance hypothesis," *Environmental Modelling and Software*, vol. 15, no. 6-7, pp. 513–519, 2000.

[13] T. Kohonen, *Self-Organizing Maps*, 3rd ed. Berlin: Springer-Verlag, 2001.